Physics Letters B 797 (2019) 134872

Contents lists available at ScienceDirect

Physics Letters B

www.elsevier.com/locate/physletb

Dilepton photoproduction on a deuteron target

Carl E. Carlson [a,*], Vladyslav Pauk [b], Marc Vanderhaeghen [b]

[a] College of William and Mary, Physics Department, Williamsburg, VA 23187, USA
[b] Institut für Kernphysik, Cluster of Excellence PRISMA$^+$, Johannes Gutenberg-Universität, Mainz, Germany

ARTICLE INFO

Article history:
Received 31 March 2019
Received in revised form 15 August 2019
Accepted 16 August 2019
Available online 21 August 2019
Editor: W. Haxton

ABSTRACT

We investigate the sensitivity of the cross section for lepton pair production off a deuteron target, $\gamma d \to l^+ l^- d$, to the deuteron charge radius. We show that for small momentum transfers the Bethe-Heitler process dominates, and that it is sensitive to the charge radius such that a cross section ratio measurement of about 0.1% relative accuracy could give a deuteron charge radius more accurate than the current electron scattering value and sufficiently accurate to distinguish between the electronic and muonic atomic values.

Over the past decade, the extractions of the proton charge radius from the Lamb shift measurements in muonic hydrogen [1, 2] resulted in a significant discrepancy in comparison with measurements with electrons [3–5], amounting to a 5.6 σ difference according to a recent re-evaluation [6]. The resolution of this "proton radius puzzle" has triggered a lot of activity, see e.g. Refs. [7–9] for recent reviews. Corresponding measurements on the deuteron have not only confirmed the puzzle [10], but have also revealed a 3.5 σ difference between the spectroscopic measurements in muonic versus ordinary deuterium. The deuteron charge radius as extracted from elastic electron scattering [11] has at present a too large error bar to distinguish between both spectroscopic values. In this letter, we investigate the sensitivity of the complementary lepton pair production process off a deuteron target, $\gamma d \to l^+ l^- d$, to the deuteron charge radius.

We consider $\gamma d \to l^- l^+ d$ in the limit of very small spacelike momentum transfer, defined as $\Delta \equiv p' - p$, with four-momenta as indicated on Fig. 1. Furthermore, we will use in the following the Mandelstam invariant $s = (k+p)^2 = M_d^2 + 2M_d E_\gamma$, with M_d the deuteron mass and E_γ the photon *lab* energy, the Mandelstam invariant $t = \Delta^2$, as well as the squared invariant mass of the lepton pair, defined as $M_{ll}^2 \equiv (l_- + l_+)^2$. In the limit of small $-t$, the Bethe-Heitler (BH) mechanism, shown in Fig. 1 dominates the cross section of the $\gamma d \to l^- l^+ d$ reaction, as we shall show.

The deuteron electromagnetic structure entering the hadronic vertex in the BH process of Fig. 1 is described by three elastic electromagnetic form factors (FFs), corresponding to the Coulomb

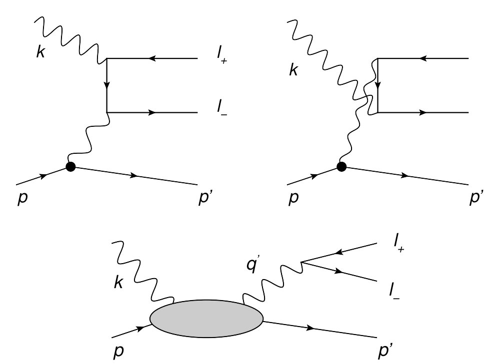

Fig. 1. Mechanisms for $\gamma d \to l^- l^+ d$. The momenta of the external particles are k for the photon, $p(p')$ for initial (final) deuterons, and l_-, l_+ for the lepton pair. The upper diagrams show the Bethe-Heitler mechanism; the lower diagram shows the Compton mechanism.

monopole (G_C), magnetic dipole (G_M), and Coulomb quadrupole (G_Q) FFs, respectively. The definitions and normalizations of G_C, G_M, and G_Q are given by [12],

$$\langle p', \lambda' | J^\mu(0) | p, \lambda \rangle = \varepsilon_\alpha(p, \lambda)\, \varepsilon^*_\beta(p', \lambda') \Big\{ -g^{\alpha\beta}\, 2P^\mu G_1(t) - \left(g^{\alpha\mu} \Delta^\beta - g^{\beta\mu} \Delta^\alpha \right) G_M(t) + \Delta^\alpha \Delta^\beta \frac{P^\mu}{M_d^2} G_3(t) \Big\}, \tag{1}$$

where $P = (p + p')/2$, ε_α and ε^*_β are deuteron polarization vectors, and the charge and quadrupole FFs are

$$G_C = G_1 + \frac{2}{3}\tau_d G_Q, \quad G_Q = G_1 - G_M + (1 + \tau_d) G_3, \tag{2}$$

* Corresponding author.
E-mail address: carlson@physics.wm.edu (C.E. Carlson).

https://doi.org/10.1016/j.physletb.2019.134872
0370-2693/

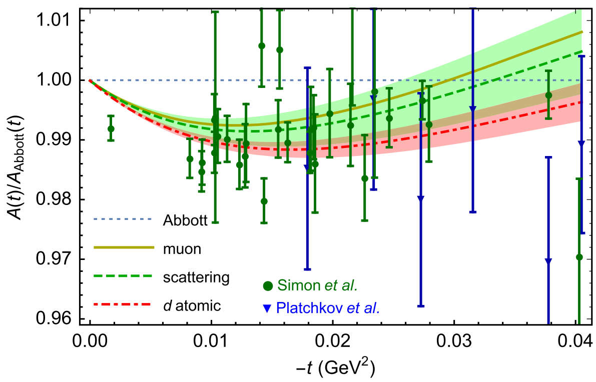

Fig. 2. Three predicted results for *ed* elastic scattering normalized to the Abbott et al. parameterization [13], with data from Simon et al. [17] and Platchkov et al. [18]. The deuteron charge radii are from the muonic deuterium Lamb shift [10] (gold solid line, with uncertainty comparable to the width of the line); from *e-d* elastic scattering [11] (green dashed line, with uncertainty limits indicated by the green band); from deuterium atomic spectroscopy [15] (red dot-dashed line, with uncertainty limits indicated by the red band). The CODATA deuteron radius [5] would be identical, on this scale, to the red dot-dashed line but with an uncertainty band 5/9 as wide. The data were given the McKinley-Feshbach [19] two photon corrections.

with normalizations $G_C(0) = 1$, $G_M(0) = \mu_d$ (magnetic moment in units $e/(2M_d)$), $G_Q(0) = Q_d$ (quadrupole moment in units e/M_d^2), and where $\tau_d \equiv -t/(4M_d^2)$. For numerical evaluation, we will use the parameterization of the deuteron FFs, obtained from scattering and tensor polarization data, and given as fit II by Abbott et al. [13]; see also [14] for details. In addition, we have the deuteron FF parameterization based on scattering data, but including a treatment of two and more photon exchange corrections, by Sick and Trautmann [11].

As the momentum transfer t is the argument appearing in the form factor (FF) in the BH process, a measurement of the cross section in the small $-t$ kinematic regime, where the BH process dominates, will allow accessing the deuteron charge FF G_C at small spacelike momentum transfer. The deuteron charge radius R_d is determined from G_C through

$$G_C(t) = 1 + \frac{1}{6} R_d^2 t + \mathscr{O}(t^2). \tag{3}$$

We quote several current values for the deuteron charge radius R_d, all in femtometers.

$$R_d = \begin{cases} 2.088 & \text{Abbott et al. fit [13]}, \\ 2.130(10) & e\text{-}d \text{ elastic scattering [11]}, \\ 2.1415(45) & \text{atomic deuterium spectroscopy [15]}, \\ 2.1413(25) & \text{CODATA 2014 [5]}, \\ 2.12562(78) & \mu\text{-}d \text{ Lamb shift [10]}, \\ 2.12771(22) & \mu\text{-}H \text{ Lamb shift \& isotope shift [10]}. \end{cases} \tag{4}$$

Of the two purely or mainly atomic values, atomic deuteron spectroscopy uses only fits to energy splittings measured in deuterium, while CODATA uses the proton radius obtained electronically and the isotope shift (the very accurate measurement of $R_d^2 - R_p^2$ [16], using ordinary hydrogen). The last listed radius measurement also uses the isotope shift, this time combined, supposing the absence of new physics, with the proton radius measured from the muonic hydrogen Lamb shift. Notable is the definite incompatibility between the deuteron radius measured using ordinary and muonic atoms.

As a preliminary observation, the effect of the radius modifications on the calculated *e-d* elastic scattering cross section is shown in Fig. 2, where cross sections are shown relative to the Abbott et al. results. Results using the Sick-Trautmann parameterization are labeled scattering, and results obtained for other values of R_d are obtained by modifying the Sick-Trautmann G_C form factor as,

$$G_C(t) = \frac{G_{C,\,\text{Sick-Trautmann}}(t)}{\left[1 - \frac{1}{6}(R_d^2 - R^2_{d,\,\text{Sick-Trautmann}})\,t\right]}. \tag{5}$$

This will allow studying the dependence on R_d. The curvature visible in the Fig. comes from the Sick-Trautmann parameterization of G_C; the correction terms in the denominator above change the slope but are too small to change the curvature visibly over the $|t|$ range we show.

The elastic cross sections are obtained from the no structure cross section and the form factors as [12]

$$\frac{d\sigma}{d\Omega} = \left.\frac{d\sigma}{d\Omega}\right|_{\text{NS}} \left[A(t) + B(t)\tan^2(\theta_e/2)\right], \tag{6}$$

with θ_e the electron lab scattering angle, and where

$$A(t) = G_C^2(t) + \frac{2}{3}\tau_d G_M^2(t) + \frac{8}{9}\tau_d^2 G_Q^2(t),$$
$$B(t) = \frac{4}{3}\tau_d\,(1+\tau_d)\,G_M^2(t). \tag{7}$$

Experimental data for Simon et al. [17] and Platchkov et al. [18] are also shown. The two photon corrections as given by McKinley and Feshbach [19] have been applied to the data.

Turning to leptoproduction, the differential cross section for the BH process is strongly peaked for leptons emitted in the incoming photon direction, and as we aim to maximize the BH contribution in this work in order to access G_C, we will study the $\gamma d \to l^- l^+ d$ process when (only) detecting the recoiling deuteron's momentum and angle, thus effectively integrating over the large lepton peak regions. The *lab* momentum of the deuteron is in one-to-one relation with the momentum transfer t: $|\vec{p}\,'|^{lab} = 2M_d\sqrt{\tau_d(1+\tau_d)}$. Furthermore, for a fixed value of t, the recoiling deuteron *lab* angle Θ_d^{lab} is expressed in terms of invariants as

$$\cos\Theta_d^{lab} = \frac{M_{ll}^2 + 2(s + M_d^2)\tau_d}{2(s - M_d^2)\sqrt{\tau_d(1+\tau_d)}}. \tag{8}$$

The differential cross section for the dominating BH process to the $\gamma d \to l^- l^+ d$ reaction, differential in t, M_{ll}^2, and the lepton solid angle $\Omega^{l^- l^+ \text{cm}}$ in the c.m. frame of the dilepton pair is given by

$$\frac{d\sigma^{BH}}{dt\,dM_{ll}^2\,d\Omega^{l^-l^+\text{cm}}} = \frac{\alpha^3\beta}{16\pi\,(s - M_d^2)^2\,t^2} L_{\mu\nu}H^{\mu\nu}, \tag{9}$$

with $\alpha \equiv e^2/4\pi \approx 1/137$, and $\beta \equiv \sqrt{1 - 4m^2/M_{ll}^2}$ the lepton velocity in the $l^- l^+$ *c.m.* frame, with m the lepton mass. Furthermore in Eq. (9), $L_{\mu\nu}$ is the unpolarized lepton tensor, averaged over the initial photon polarizations, given by

$$L_{\mu\nu} = -\frac{1}{2}\text{Tr}\left\{(\not{l}_- + m)\left[\gamma^\alpha \frac{\not{l}_- - \not{k} + m}{-2k\cdot l_-}\gamma_\mu + \gamma_\mu \frac{\not{k} - \not{l}_+ + m}{-2k\cdot l_+}\gamma^\alpha\right]\right.$$
$$\left. \times\,(\not{l}_+ - m)\left[\gamma_\nu \frac{\not{l}_- - \not{k} + m}{-2k\cdot l_-}\gamma_\alpha + \gamma_\alpha \frac{\not{k} - \not{l}_+ + m}{-2k\cdot l_+}\gamma_\nu\right]\right\}, \tag{10}$$

and $H^{\mu\nu}$ is the unpolarized hadronic tensor defined by

$$H^{\mu\nu} = \frac{1}{3}\sum_{\lambda=0,\pm1}\sum_{\lambda'=0,\pm1}\langle p',\lambda'|\,J^\mu(0)\,|p,\lambda\rangle$$
$$\times\,\langle p',\lambda'|\,J^\nu(0)\,|p,\lambda\rangle^*. \tag{11}$$

Using Eq. (1), the hadronic tensor for the BH process can be expressed as

$$H^{\mu\nu} = \left(-g^{\mu\nu} + \frac{\Delta^\mu \Delta^\nu}{\Delta^2}\right)\left[\frac{8}{3}M_d^2 \tau_d (1+\tau_d)\, G_M^2\right] + 4\, P^\mu P^\nu \left[G_C^2 + \frac{2}{3}\tau_d\, G_M^2 + \frac{8}{9}\tau_d^2\, G_Q^2\right], \tag{12}$$

and the FFs are functions of the momentum transfer t.

When detecting only the deuteron momentum and angle, the cross section integrated over the lepton angles is

$$\frac{d\sigma^{BH}}{dt\, dM_{ll}^2} = \frac{4\alpha^3 \beta}{(s-M_d^2)^2 t^2 (M_{ll}^2 - t)^4} \times \left\{C_E\left(G_C^2 + \frac{8}{9}\tau_d^2 G_Q^2\right) + C_M \frac{2}{3}\tau_d G_M^2\right\}, \tag{13}$$

where

$$C_{E,M} = C_{E,M}^{(1)} + C_{E,M}^{(2)} \frac{1}{\beta} \ln\left(\frac{1+\beta}{1-\beta}\right). \tag{14}$$

The coefficients $C_{E,M}^{(1)}$, and $C_{E,M}^{(2)}$ are expressed through invariants as

$$\begin{aligned}
C_E^{(1)} &= t\left(s - M_d^2\right)\left(s - M_d^2 - M_{ll}^2 + t\right) \\
&\quad \times \left[M_{ll}^4 + 6M_{ll}^2 t + t^2 + 4m^2 M_{ll}^2\right] \\
&\quad + \left(M_{ll}^2 - t\right)^2 \left[t^2 M_{ll}^2 + M_d^2 (M_{ll}^2 + t)^2 + 4m^2 M_d^2 M_{ll}^2\right], \\
C_E^{(2)} &= -t\left(s - M_d^2\right)\left(s - M_d^2 - M_{ll}^2 + t\right) \\
&\quad \times \left[M_{ll}^4 + t^2 + 4m^2\left(M_{ll}^2 + 2t - 2m^2\right)\right] \\
&\quad + \left(M_{ll}^2 - t\right)^2 \\
&\quad \times \left[-M_d^2 (M_{ll}^4 + t^2) + 2m^2\left(-t^2 - 2M_d^2 M_{ll}^2 + 4m^2 M_d^2\right)\right], \\
C_M^{(1)} &= C_E^{(1)} - 2M_d^2(1+\tau_d)\left(M_{ll}^2 - t\right)^2 \left[M_{ll}^4 + t^2 + 4m^2 M_{ll}^2\right], \\
C_M^{(2)} &= C_E^{(2)} + 2M_d^2(1+\tau_d)\left(M_{ll}^2 - t\right)^2 \\
&\quad \times \left[M_{ll}^4 + t^2 + 4m^2\left(M_{ll}^2 - t - 2m^2\right)\right].
\end{aligned} \tag{15}$$

The absolute Bethe-Heitler cross sections are shown in Fig. 3. The abscissa is the dilepton mass-squared M_{ll}^2, with both electrons and muons represented, and showing three different values of $-t$. The plot is similar to the one for protons [20], but the cross sections are smaller because of the faster falloff with $|t|$ of the deuteron FFs.

To estimate the Compton mechanism, the lower graph in Fig. 1, we estimate the S-matrix amplitude

$$\begin{aligned}
\mathscr{M}_C &= -\frac{e^3}{q'^2}\epsilon_\nu(k,\lambda_\gamma)\bar{u}(l_-,s_-)\gamma_\mu v(l_+,s_+) \\
&\quad \times \int d^4x\, e^{iq'x}\langle p',\lambda'|T\, J^\mu(x) J^\nu(0)|p,\lambda\rangle \\
&\equiv -i\frac{e}{q'^2}\epsilon_\nu(k,\lambda_\gamma)\bar{u}(l_-,s_-)\gamma_\mu v(l_+,s_+)\, 8\pi M_d T_{\rm TCS}^{\mu\nu}(k,q',P),
\end{aligned} \tag{16}$$

where $T_{\rm TCS}^{\mu\nu}$ is the unpolarized timelike real Compton tensor and λ_γ is the photon polarization.

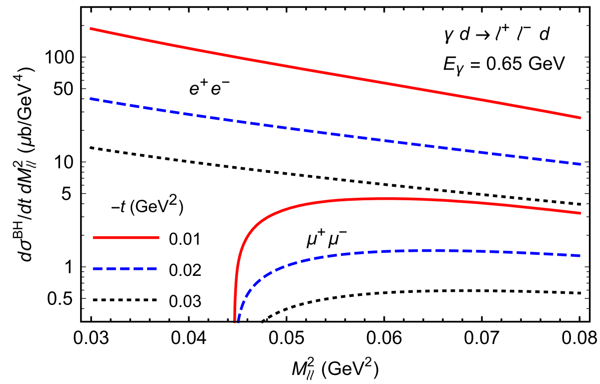

Fig. 3. Absolute cross sections, using the Abbott et al. [13] deuteron FFs, showing the lepton pair invariant mass dependence of the $\gamma d \to e^+e^- d$ process (upper three curves) and the $\gamma d \to \mu^+\mu^- d$ process (lower three curves) at $E_\gamma = 0.65$ GeV. Three values of the momentum transfer are shown.

For near-real, near-forward kinematics, $M_{ll}^2, |t| \ll s$ the unpolarized TCS amplitude can be approximated by,

$$T_{\rm TCS}^{\mu\nu}(k,q',P) \approx \left(g^{\mu\nu} - \frac{q'^\mu k^\nu}{q'\cdot k}\right) T_{1d}(\nu,t,M_{ll}^2), \tag{17}$$

where T_{1d} denotes the leading scalar amplitude, and ν the crossing symmetric variable, $\nu = E_\gamma - (q'^2 - t)/(4M_d)$.

For $M_{ll}^2, |t| \ll s$, we can further approximate

$$T_{1d}(\nu,t,q'^2) \approx f(\nu), \tag{18}$$

where $f(\nu)$ is the unpolarized forward real Compton amplitude for a deuteron target. Its imaginary part can be obtained from the photoproduction total cross section, or from the $F_{1d}(\nu,Q^2)$ structure function, as

$$\mathrm{Im}\, f(\nu) = \frac{\nu}{4\pi}\sigma(\nu) = \frac{\pi\alpha}{M_d}F_{1d}(\nu,0). \tag{19}$$

Analyticity and the low-energy theorem value of $f(0)$ allow us to obtain the real part of f from a once-subtracted dispersion relation,

$$\mathrm{Re}\, f(\nu) = -\frac{\alpha}{M_d} + \frac{\nu^2}{2\pi^2}\,\fint_{\nu_0}^{\infty} d\nu' \frac{\sigma(\nu')}{\nu'^2 - \nu^2}, \tag{20}$$

where ν_0 is the inelastic threshold, $\nu_0 = ((M_n + M_p)^2 - M_d^2)/(2M_d) \approx 2.23$ MeV.

The Compton contribution to the $\gamma d \to l^+l^- d$ differential cross section, integrated over lepton angles, is

$$\frac{d\sigma^{\rm TCS}}{dt\, dM_{ll}^2} = \frac{2M_d^2 \alpha^3 \beta}{(s-M_d^2)^2 M_{ll}^2}\left(1 - \frac{\beta^2}{3}\right)\left|\frac{f(\nu)}{\alpha}\right|^2. \tag{21}$$

Fig. 4 shows the Compton cross section, compared to the Bethe-Heitler, for particular values of t and M_{ll}^2, with E_γ on the abscissa. We obtained $\sigma(\nu)$, or $F_{1d}(\nu,0)$ in the quasi-elastic region from the fits of [21], and in the nucleon inelastic region from Bosted-Christy [22] deuteron fits when $s_{\rm nucleon} < (3.1\ \mathrm{GeV})^2$ and from Capella et al. [23], isospin modified for the neutron, above that. At leading order in α, there is no interference between the Compton and Bethe-Heitler contributions when we integrate over the lepton angles. The Compton cross section is more than two orders of magnitude smaller than the Bethe-Heitler cross section, for this energy and momentum transfer range.

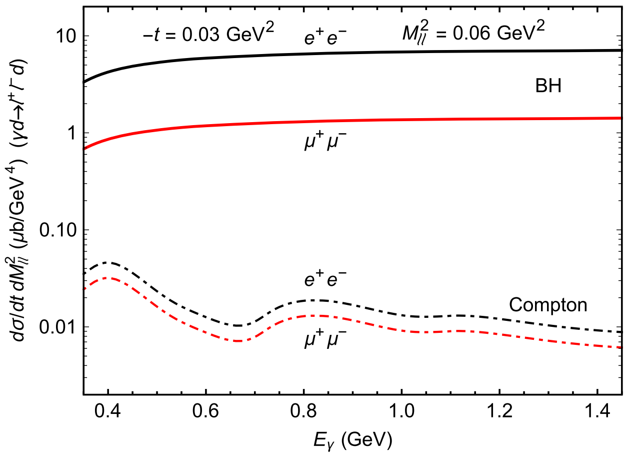

Fig. 4. The differential cross section for $\gamma d \to l^+l^-d$ plotted vs. E_γ and showing both the Bethe-Heitler and Compton contributions, for values of t and dilepton mass indicated.

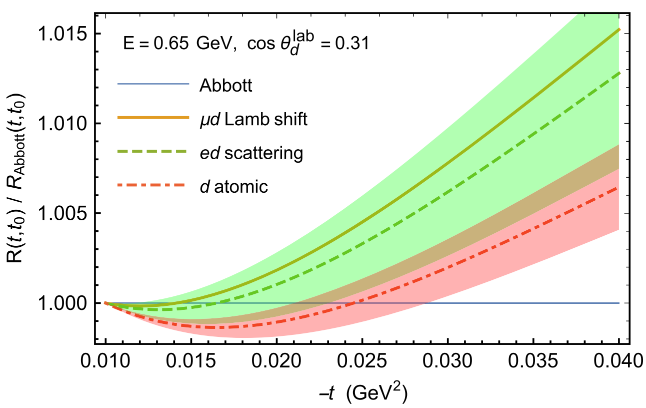

Fig. 5. The t-dependence of the $\gamma d \to e^+e^-d$ cross section, $R(t,t_0) \equiv d\sigma/dt\,dM_{ll}^2(t)/d\sigma/dt\,dM_{ll}^2(t_0)$, relative to a reference value $t_0 = -0.01$ GeV^2, at fixed outgoing deuteron lab angle, for beam energy 0.65 GeV. The ratio is normalized to the result for Abbott et al. FFs [13]. The different deuteron radii and associated error bands are as in Fig. 2.

The sensitivity of the differential inelastic cross section for different FFs and different deuteron radii is shown in Fig. 5, as a function of $-t$, with a photon beam energy 0.65 GeV, corresponding with a minimum in the Compton contribution. The plot shows the cross section relative to a reference value $t_0 = -0.01$ GeV^2, and normalized to results from the Abbott et al. parameterization. The outgoing deuteron angle has been fixed.

The curves shown are examples based on a particular fit (Eq. (5) and Ref. [11]) to existing elastic scattering data. Other authors present other acceptable fits to the same data (for example see [24]), and using these can change to some extent the slope and curvature of the lines seen in the Figure, although without changing their relative position or spacings. When data for lepton-pair photoproduction is available, one will fit to obtain the physical curvature and slope, irrespective of earlier fits. The Fig. here is shown to argue that anticipatable accuracy will allow distinguishing among the deuteron radius values currently plausible.

The different radii give curves on the right hand part of Fig. 5 that differ by several times 0.1%, so that measurements of the plotted ratio at different t with 0.1% relative accuracy would allow distinguishing the various fits. There are experiments that anticipate that level of accuracy now in related circumstances. A particular example is a proposed electron-proton scattering experiment at MAMI [25], where the recoil proton energy and angle is to be measured with an active hydrogen target, at momentum transfers comparable to ours. The point to point accuracy anticipated is 0.1% in the cross sections, the same as needed here.

Additionally, the fixed angle here can allow better experimental calibration than in an elastic scattering experiment, where different momentum transfers require different scattering angles, for a given beam energy. Further, the one-loop radiative corrections to the dilepton production have been recently evaluated in the kinematics discussed in the present work [26,27]. In the t-range shown in Fig. 5, the dilepton mass varies in the range $0.027 \lesssim M_{ll}^2 \lesssim 0.030$ GeV^2. Over this kinematic range, the radiative correction factor changes by an amount at the 0.1% level (see Fig. 13 in Ref. [27]). As only this variation is of relevance for the ratio plotted in Fig. 5, we can safely assert that within the error bands shown in the figure, the radiative corrections do not affect the result.

In this work we have studied dilepton photoproduction off a deuteron with the aim of extracting the deuteron charge radius. By studying the momentum transfer dependence of the outgoing deuteron at a fixed angle, we have seen that a cross section ratio measurement of about 0.1% accuracy will allow extracting a deuteron charge radius more accurate than the present value from elastic scattering, and can distinguish between the values obtained from ordinary and muonic deuterium, which are currently at variance by around 3.5 σ.

Acknowledgements

We thank Keith Griffioen and Tim Hayward for useful conversations, and Ingo Sick for providing details of the fits in [11]. CEC thanks the National Science Foundation (USA) for support under grants PHY-1516509 and PHY-1812326, and the Johannes Gutenberg-University, Mainz, for hospitality while this work was completed. The work of VP and MV was supported by the Deutsche Forschungsgemeinschaft (DFG, German Research Foundation), in part through the Collaborative Research Center [The Low-Energy Frontier of the Standard Model, Projektnummer 204404729 - SFB 1044], and in part through the Cluster of Excellence [Precision Physics, Fundamental Interactions, and Structure of Matter] (PRISMA$^+$ EXC 2118/1) within the German Excellence Strategy (Project ID 39083149).

References

[1] R. Pohl, et al., Nature 466 (2010) 213.
[2] A. Antognini, et al., Science 339 (2013) 417.
[3] J.C. Bernauer, et al., A1, Phys. Rev. Lett. 105 (2010) 242001.
[4] J.C. Bernauer, et al., A1, Phys. Rev. C 90 (2014) 015206.
[5] P.J. Mohr, D.B. Newell, B.N. Taylor, Rev. Mod. Phys. 88 (2016) 035009.
[6] J.J. Krauth, et al., in: Proceedings, 52nd Rencontres de Moriond on Electroweak Interactions and Unified Theories, La Thuile, Italy, March 18–25, 2017, 2017, pp. 95–102.
[7] R. Pohl, R. Gilman, G.A. Miller, K. Pachucki, Annu. Rev. Nucl. Part. Sci. 63 (2013) 175.
[8] C.E. Carlson, Prog. Part. Nucl. Phys. 82 (2015) 59.
[9] R.J. Hill, in: Proceedings, 12th Conference on Quark Confinement and the Hadron Spectrum (Confinement XII), Thessaloniki, Greece, EPJ Web Conf. 137 (2017) 01023.
[10] R. Pohl, et al., CREMA, Science 353 (2016) 669.
[11] I. Sick, D. Trautmann, Nucl. Phys. A 637 (1998) 559.
[12] R.G. Arnold, C.E. Carlson, F. Gross, Phys. Rev. C 21 (1980) 1426.
[13] D. Abbott, et al., JLAB t20, Eur. Phys. J. A 7 (2000) 421.
[14] C.E. Carlson, M. Vanderhaeghen, Eur. Phys. J. A 41 (2009) 1.
[15] R. Pohl, et al., Metrologia 54 (2017) L1.
[16] C.G. Parthey, A. Matveev, J. Alnis, R. Pohl, T. Udem, U.D. Jentschura, N. Kolachevsky, T.W. Hänsch, Phys. Rev. Lett. 104 (2010) 233001.

[17] G.G. Simon, C. Schmitt, V.H. Walther, Nucl. Phys. A 364 (1981) 285.
[18] S. Platchkov, et al., Nucl. Phys. A 510 (1990) 740.
[19] W.A. McKinley, H. Feshbach, Phys. Rev. 74 (1948) 1759.
[20] V. Pauk, M. Vanderhaeghen, Phys. Rev. Lett. 115 (2015) 221804.
[21] C.E. Carlson, M. Gorchtein, M. Vanderhaeghen, Phys. Rev. A 89 (2014) 022504.
[22] P.E. Bosted, M.E. Christy, Phys. Rev. C 77 (2008) 065206.
[23] A. Capella, A. Kaidalov, C. Merino, J. Tran Thanh Van, Phys. Lett. B 337 (1994) 358.
[24] T.B. Hayward, K.A. Griffioen, arXiv:1804.09150 [nucl-ex], 2018.
[25] A. Vorobyev, A. Denig, Spokespersons for proposal MAMI-A2, www.blogs.uni-mainz.de/fb08-mami-experiments/files/2017/11/ep_-proposal.pdf.
[26] M. Heller, O. Tomalak, M. Vanderhaeghen, Phys. Rev. D 97 (2018) 076012.
[27] M. Heller, O. Tomalak, M. Vanderhaeghen, S. Wu, arXiv:1906.02706 [hep-ph], 2019.